RESEARCH PAPER

siRNA-FAM and Paclitaxel delivery to MCF-7 cells via folic acid-PLA-Spermine-PEG-Fe 3 O 4 nanoparticles

Sahar Mohajeri[1]*, Hashem Yaghoubi[2*]

[1]Department of Chemistry, Ard.C., Islamic Azad University, Ardabil, Iran
[2]Department of Biology, Ard.C., Islamic Azad University, Ardabil, Iran

Abstract

Objective(s): An effective targeted cancer therapy should maximize drug accumulation within tumors while minimizing off-target effects on healthy tissues. Folate receptors, frequently overexpressed in various malignancies, render folic acid a promising targeting ligand for nanoparticle-mediated drug delivery.

Materials and Methods: For this study, folic acid (FA)-modified PLA-spermine-PEG-Fe_3O_4 nanoparticles were synthesized. These multifunctional nanoparticles were employed for the co-delivery of siRNA and paclitaxel (PTX) to targeted sites. The structural and morphological properties of the fabricated nanoparticles were characterized using Fourier transform infrared spectroscopy (FTIR), thermogravimetric analysis (TGA), vibrating sample magnetometry (VSM), scanning electron microscopy (SEM), transmission electron microscopy (TEM), and dynamic light scattering (DLS).

Results: TGA and FTIR analyses confirmed the successful synthesis of the PLA-spermine-PEG-FA (FPSP) copolymer. TEM and SEM imaging revealed that the FPSPFe/siRNA-FAM/PTX micelles possessed a smooth, spherical morphology. Additionally, VSM measurements indicated that the micelles exhibited suitable magnetic properties at room temperature. The drug release behavior of the FPSPFe/siRNA-FAM/PTX micelles was evaluated under both neutral and acidic conditions, demonstrating accelerated release under acidic pH conditions. The MTT assay demonstrated good biocompatibility of the micelles, while flow cytometry confirmed their ability to effectively deliver siRNA-FAM and PTX.

Conclusion: The results demonstrated the high efficiency of FPSPFe/siRNA-FAM/PTX micelles in delivering both PTX and siRNA-FAM to MCF-7 cancer cells simultaneously.

Keywords: *Drug delivery systems, Folic acid receptor, MCF-7 cells, Magnetic iron oxide nanoparticles, Paclitaxel, RNA small interfering agent*

How to cite this article

Mohajeri S, Yaghoubi H. siRNA-FAM and Paclitaxel Delivery to MCF-7 Cells via Folic acid-PLA-Spermine-PEG-Fe3O4. Nanomed J. 2025; 12: 1-. DOI: 10.22038/NMJ.2025.85959.2154

Abbreviations

3-[4,5-dimethylthiazol-2-yl]-2,5-diphenyl tetrazolium bromide: MTT
Bovine serum albumin: BSA
Breast cancer: BC
Dulbecco's Modified Eagle Medium: DMEM
Dynamic Light Scattering: DLS
Fetal Bovine Serum: FBS
Folate receptors: FRs
Folic Acid: FA
Folic acid: FA
Fourier Transform Infrared Spectroscopy: FTIR
Human serum albumin: HSA
IC_{50}: Half-maximal inhibitory concentration
Iron oxide nanoparticles: Fe_3O_4 NPs
Messenger RNA: mRNA
Molecular weight: MW
Nanoparticle: NP
Paclitaxel: PTX
Phosphate Buffered saline: PBS
PLA-spermine-PEG-FA: FPSP
PLA-spermine-PEG-FA-Fe_3O_4: FPSPFe
Poly (DL-lactic-co-glycolic acid): PLGA
Polylactic acid: PLA
Polyethylene glycol: PEG
Poly-Vinyl Alcohol: PVA
Poly-Vinyl Pyrrolidone: PVP
Reticuloendothelial system: RES
Ribonuclease A: RNase A
RNA interference: RNAi
Scanning Electron Microscopy: SEM
Small interfering RNA: siRNA
Thermo Gravimetric Analysis: TGA
Transmission Electron Microscopy: TEM
Vibrating Sample Magnetometer: VSM

**Corresponding author(s) Email: yaghoubi_h@iau.ac.ir, sahar.mohajeri@iau.ac.ir*
Note. This manuscript was submitted on February 08, 2025; approved on June 30, 2025.

INTRODUCTION

Cancer remains one of the most pressing global public health challenges, necessitating urgent and collaborative efforts in prevention, treatment, and research [1]. According to the 2023 GLOBOCAN report on global cancer burden, breast cancer (BC) has become the most frequently diagnosed cancer among women, surpassing lung cancer [2]. Significant advancements in treatment modalities—including surgery, radiotherapy, chemotherapy, and targeted therapies—have contributed to improved overall survival rates [3].

Nanoparticle (NP)-based carriers and liposomal formulations represent recent advancements in drug delivery systems, offering enhanced therapeutic efficacy and reduced systemic toxicity [4]. Numerous studies have explored the application of nanotechnology to develop innovative delivery platforms for chemotherapeutic agents [5]. By facilitating selective drug accumulation in tumor tissues while sparing healthy cells, nanocarriers play a pivotal role in minimizing drug-associated adverse effects [6]. Biocompatible and biodegradable polymeric NPs—such as chitosan, human serum albumin (HSA), and bovine serum albumin (BSA)—have gained attention for their potential in therapeutic and receptor-mediated delivery systems [7]. Micelles, typically amphiphilic and spherical, range in size from 100 to 300 nm and are composed of either biocompatible synthetic polymers or natural macromolecules [8]. Common biodegradable polymers used in micelle formation include chitosan, polylactic acid (PLA), polyethylene glycol (PEG), and poly(DL-lactic-co-glycolic acid) (PLGA).

Polyamines are vital for maintaining cellular and physiological homeostasis [9]. They have been shown to influence the structure of macromolecules, regulate ion channels, and modulate nucleic acid and protein synthesis, as well as gene expression, protein function, and cellular defense mechanisms against oxidative stress [10]. Among them, spermine is a key polyamine in mammalian cells, playing an essential role in protein synthesis. Due to its non-toxic nature, high adsorption capacity, excellent biocompatibility and biodegradability, cost-effectiveness, rapid kinetics, and chemical versatility, spermine has attracted considerable interest as a functional component in biomedical applications [11]. The presence of multiple amine groups in certain compounds facilitates strong electrostatic interactions with siRNA, leading to the formation of compact nanoparticles that protect the genetic material from enzymatic degradation [12]. These siRNA-loaded complexes exhibit enhanced cellular uptake compared to naked siRNA, partly due to spermine's capacity to interact with cellular membranes [13]. Surface functionalization of nanoparticles with biocompatible, hydrophilic, and neutral polymers improves their solubility in the bloodstream and minimizes undesirable interactions with plasma polyanions [14]. Amphiphilic segmental copolymers, which comprise both hydrophilic and hydrophobic segments, have recently garnered considerable attention due to their potential in drug delivery applications and their unique phase behavior in aqueous environments [11]. Due to their broad polarity range and solubility in diverse solvents, these copolymers can self-assemble into various nanostructures depending on solvent characteristics and copolymer composition [15].

Polyethylene glycol (PEG) and polylactic acid (PLA) are widely utilized biocompatible polymers in biomedical applications due to their non-toxic nature and favorable biodegradability profiles [16]. PEG, a nonionic polyether, is particularly prominent in pharmaceutical formulations, as it reduces immunogenicity and prolongs systemic circulation of therapeutic agents [16]. By shielding drugs from proteolytic degradation and increasing their molecular weight (MW), PEG alters pharmacokinetics and decreases renal clearance rates [17]. Moreover, PEG enhances drug solubility by forming a hydration shell around the polymer, thereby improving the aqueous dispersibility of the drug.

Iron oxide nanoparticles (Fe_3O_4 NPs) have gained attention as promising nanocarriers for targeted drug and gene delivery—especially for small interfering RNAs (siRNAs)—due to their unique features, including excellent biocompatibility, superparamagnetic behavior, and highly tunable surface chemistry [18]. These nanoparticles are capable of overcoming key therapeutic challenges such as rapid siRNA degradation, nonspecific cellular uptake, and poor endosomal escape, thereby markedly enhancing the overall efficiency of RNA interference (RNAi)-based therapies [19]. Fe_3O_4 nanoparticles offer superior targeting efficiency compared to non-magnetic delivery systems, as they respond to external magnetic fields, enabling precise spatial control and active guidance to tumor sites. In contrast to passive carriers that rely solely on the enhanced permeability and retention (EPR) effect, Fe_3O_4-based systems can overcome physiological barriers such as blood flow, thereby facilitating enhanced local drug accumulation. Furthermore, their surface can be functionalized with targeting

ligands (e.g., antibodies), enabling dual active–passive targeting strategies that significantly improve delivery specificity [18]. Previous studies have demonstrated that nanoparticles targeted to receptors overexpressed on cancer cells—such as folate receptors (FRs)—can enhance accumulation in tumor tissues while minimizing distribution to healthy organs [20]. Folic acid (FA) has emerged as a key targeting ligand for siRNA delivery due to its high binding affinity for FRs, which are abundantly expressed in various cancers and inflammatory cells but show limited expression in normal tissues [21]. Notably, FR expression in MCF-7 breast cancer cells is approximately eight times higher than in normal mammary epithelial cells ($p < 0.01$) [22]. Conjugation of FA to nanocarriers—including liposomes, polymers, or inorganic nanoparticles—enables the selective delivery of siRNA to FR-positive cells via receptor-mediated endocytosis, thereby enhancing intracellular uptake and reducing off-target effects [23]. This targeted approach enhances gene silencing efficacy while reducing systemic toxicity, capitalizing on the inherent biocompatibility and low immunogenicity of FA [24]. Consequently, FA-functionalized lipid and polymer-based nanoparticles have been widely utilized to achieve precise targeting of cancer cells in drug delivery applications.

The incorporation of cationic spermine into an amphiphilic PLA–PEG framework, functionalized with folic acid (FA), offers a multifaceted solution to key limitations in combinatorial cancer therapy. The protonatable amine groups of spermine facilitate electrostatic complexation with siRNA, thereby shielding it from enzymatic degradation and promoting endosomal escape via the proton sponge effect. Concurrently, the PLA–PEG copolymer matrix serves dual functions: (i) encapsulation of hydrophobic paclitaxel (PTX) within its hydrophobic PLA core, and (ii) extension of systemic circulation time through PEG-mediated steric stabilization. This synergistically engineered nanoparticle, further enhanced by folate receptor-mediated active targeting, enables spatiotemporally controlled co-delivery of therapeutic agents [25].

Small interfering RNA (siRNA) has emerged as a powerful tool in gene delivery, particularly in the context of cancer therapy. Operating through the RNA interference (RNAi) pathway, siRNA leverages the cell's endogenous machinery to degrade specific messenger RNA (mRNA) molecules, thereby silencing the expression of genes implicated in carcinogenesis [26]. This targeted approach holds substantial promise for cancer prevention and treatment by enabling precise downregulation of oncogenes and upregulation of tumor suppressor genes [27]. Advances in delivery technologies—such as viral vectors and lipid-based nanoparticles—have further enhanced the stability and bioavailability of siRNAs *in vivo*, significantly increasing their therapeutic potential [26]. Continued research into siRNA-based therapeutics not only paves the way for innovative cancer treatments but also aligns with the vision of personalized medicine, where therapeutic regimens are tailored to the unique genetic profile of individual tumors [28].

Paclitaxel (PTX), a widely used chemotherapeutic agent originally isolated from the bark of the Pacific yew tree, has become a cornerstone in the treatment of several malignancies, including ovarian, breast, and lung cancers [29]. Its anticancer activity primarily stems from its ability to stabilize microtubules, thereby disrupting mitotic spindle formation and effectively inhibiting cell division [30]. This mechanism not only suppresses tumor cell proliferation but also induces apoptosis, ultimately contributing to tumor regression [28]. Extensive clinical trials have validated PTX as a key component in combination chemotherapy regimens, leading to improved overall survival and enhanced quality of life in cancer patients [31]. Nonetheless, its clinical use is frequently associated with notable adverse effects, necessitating careful patient monitoring and supportive care.

Combination therapy, which involves the use of multiple therapeutic agents with complementary mechanisms of action, has emerged as a promising strategy to enhance treatment efficacy and overcome drug resistance in oncology. By simultaneously targeting distinct molecular pathways, this approach enhances therapeutic synergy and reduces the likelihood of resistance development [32]. The co-delivery of siRNA and PTX exemplifies a novel therapeutic paradigm that leverages the mechanistic complementarity of these two agents. While PTX induces G2/M phase cell cycle arrest through microtubule stabilization, siRNA enables precise gene silencing of targets implicated in tumor progression, such as antiapoptotic proteins and chemoresistance-related genes [33]. This multifaceted strategy promotes tumor cell apoptosis via synergistic mechanisms and addresses one of the major obstacles in cancer therapy: the emergence of treatment resistance.

Amid continued advancements in formulation strategies and delivery platforms, paclitaxel (PTX)

remains a cornerstone of oncologic treatment with expanding potential in cancer therapeutics.

In this study, we investigated the therapeutic efficacy of folic acid (FA)-functionalized PLA–spermine–PEG–Fe_3O_4 polymeric nanoparticles for the targeted co-delivery of PTX and siRNA. Following successful synthesis and physicochemical characterization of the nanocarriers, their impact on the proliferation and viability of MCF-7 breast cancer cells was systematically evaluated.

MATERIALS AND METHODS

Preparation of Methanolic Extracts from Silybum marianum Plants

The methanolic extract of *Silybum marianum* was prepared by adding 10 g of powdered leaves to 100 mL of 80% methanol. The mixture was subjected to sonication at 30 kHz and 150 W for 10 minutes, followed by continuous shaking at 37 °C for 24 hours. The resulting extract was then centrifuged to remove plant debris and subsequently filtered through standard filter paper to obtain a clear methanolic extract [34].

Green synthesis of iron oxide (Fe_3O_4) nanoparticles

Fe_3O_4 nanoparticles were synthesized using a co-precipitation method. A three-necked 250 mL round-bottom flask was charged with 3.3 g of iron(III) chloride hexahydrate ($FeCl_3 \cdot 6H_2O$) and 3.3 g of iron(II) chloride tetrahydrate ($FeCl_2 \cdot 4H_2O$), followed by the addition of 100 mL of deionized water. After mounting a thermometer in one neck, nitrogen gas was purged into the system to create an inert atmosphere. The solution was stirred at 80 °C for 10 minutes. Subsequently, 15 mL of hydroalcoholic *S.marianum* extract was gradually added under continuous stirring. After 10 minutes, 60 mL of 1 M NaOH solution was introduced dropwise. The formation of Fe_3O_4 nanoparticles was indicated by a color change from brown to black. The nanoparticles were collected using an external magnet and thoroughly washed with deionized water to remove residual impurities [35].

Preparation of spermine-PLA-spermine

The spermine–PLA–spermine copolymer was synthesized via amide bond formation between the amine groups of spermine and the carboxylic acid groups of COOH–PLA–COOH, using N-hydroxysuccinimide (NHS) and 1-ethyl-3-(3-dimethylaminopropyl) carbodiimide (EDC) as coupling agents in methanol. After 2 hours of reaction, 1 mL of ethylenediamine was added to further crosslink terminal groups, and the mixture was stirred at room temperature overnight. Subsequently, the activated COOH–PLA–COOH was dissolved in dimethyl sulfoxide (DMSO), and the reaction was allowed to proceed for an additional 48 hours. The final product was purified by dialysis using a membrane with a molecular weight cutoff (MWCO) of 11 kDa for 12 hours at 4 °C against deionized water to remove unreacted species [14].

Preparation of FA-PLA-Spermine-PEG copolymer nanoparticles (FPSPs)

For nanoparticle assembly, 2 g of spermine–PLA–spermine and 4 g of COOH–PEG–FA were each dissolved separately in 20 mL of chloroform. The COOH–PEG–FA solution was then slowly added dropwise to the spermine–PLA–spermine solution under continuous stirring. The resulting mixture was stirred at 50 °C for 24 hours to facilitate conjugation. Afterward, the organic solvent was gradually replaced with methanol and subsequently with deionized water. The final product was purified by dialysis against water at 4 °C for 48 hours to remove unreacted compounds and solvent residues [36].

Preparation of FPSPFe/PTX, FPSPFe/siRNA-FAM, and FPSPFe/PTX/siRNA-FAM micelles

Micelles containing FPSPFe/PTX, FPSPFe/siRNA-FAM, and FPSPFe/PTX/siRNA-FAM were prepared using a solvent diffusion method. Briefly, 20 mg of FPSP copolymer and 2 mg of Fe_3O_4 were dissolved in 4 mL of chloroform and sonicated (60 kHz, 100 W) with 0.5 mL of an aqueous solution containing 250 µg of siRNA-FAM and 1 mg of PTX (either separately or in combination). To the resulting emulsion, 6 mL of 1% polyvinyl alcohol (PVA) solution was added, followed by an additional 2 minutes of sonication under the same conditions. Subsequently, 30 mL of 0.3% polyvinylpyrrolidone (PVP) solution was introduced into the system. After 5 hours of mixing, chloroform was removed by rotary centrifugation at 12,000 × g for 10 minutes. The nanoparticles were then collected by centrifugation at 15,000 rpm for 30 minutes, freeze-dried, and stored at –20 °C for further characterization and biological evaluation [37].

Characteristics of synthesized nanoparticles

Fourier-transform infrared spectroscopy (FTIR; ABB Bomem MB) and thermogravimetric analysis (TGA; TG-DTA-32, Japan) were performed to characterize the PSPF copolymers. TGA measurements were conducted under atmospheric air from 25°C to 600°C at a heating rate of 20°C/min. The morphological features of the synthesized nanoparticles were examined using

scanning electron microscopy (SEM) and transmission electron microscopy (TEM). Particle size distribution and zeta potential were measured using dynamic light scattering (DLS). Magnetic properties of the nanoparticles were evaluated using a vibrating sample magnetometer (VSM; Lake Shore Model 7400, Tokyo, Japan).

Determination of the drug encapsulation efficiency of synthesized nanoparticles

The encapsulation efficiency (EE%) of siRNA-FAM and paclitaxel (PTX) within FPSPFe nanoparticles was determined spectrophotometrically using a Bio-Rad SmartSpec™ Plus spectrophotometer (USA). After nanoparticle preparation, the suspension was centrifuged, and the absorbance of the resulting supernatant was measured at 230 nm for PTX and 490 nm for siRNA-FAM to quantify the unencapsulated drug. The EE% was calculated by comparing the concentration of free drug in the supernatant to the initial amount used in the loading process (1 mg), using the following equation [26]:

$$EE\% = (W_{\text{initial PTX/siRNA}} - W_{\text{free PTX/siRNA}} / W_{\text{initial PTX/siRNA}})$$

Kinetics of drug release from nanoparticles

An *in vitro* drug release study was performed under two different pH conditions (acidic and neutral) to simulate the physiological environments of cancerous and normal tissues. Nanoparticle suspensions were prepared by dispersing the samples in 10 mL of phosphate-buffered saline (PBS) at the desired pH and incubated at 37 °C for predetermined time intervals (12, 24, 36, 48, 60, and 72 hours). At each time point, the samples were centrifuged at 15,000 rpm for 30 minutes to separate the nanoparticles. The supernatant was collected to quantify the released amounts of paclitaxel (PTX) and siRNA-FAM. The nanoparticles were then re-dispersed in fresh PBS and returned to incubation until the next time point. The concentrations of PTX and siRNA-FAM in the collected supernatants were determined using the previously described spectrophotometric method [20]:

$$\text{Cumulative release percentage} = \frac{Dr^{t} + Dr^{t+1}}{DE}$$

Dr^{t}= The measured amount of drug in the supernatant at any time (t)

Dr^{t+1}= The measured amount of drug in the supernatant at time t+1;

De= The amount of drug encapsulated in the nanoparticles

Cell culture

The MCF-7 human breast cancer cell line was obtained from the American Type Culture Collection (ATCC, Manassas, VA, USA) and cultured in Dulbecco's Modified Eagle's Medium (DMEM; Sigma-Aldrich, USA) supplemented with 10% fetal bovine serum (FBS). Cells were maintained at 37 °C in a humidified incubator with 5% CO_2 and 21% O_2.

In vitro cytotoxicity studies

Cytotoxicity was assessed using the MTT assay, a colorimetric method based on the ability of metabolically active cells to reduce 3-[4,5-dimethylthiazol-2-yl]-2,5-diphenyl tetrazolium bromide (MTT) into insoluble formazan crystals, indicative of mitochondrial enzymatic activity. MCF-7 cells were seeded at a density of 7,500 cells per well into 96-well plates and incubated at 37 °C in a humidified atmosphere with 5% CO_2 for 24 hours to allow cell attachment and initial proliferation. After incubation, the culture medium was removed and replaced with fresh medium containing varying concentrations of FPSPFe/siRNA-FAM/PTX micelles, corresponding to PTX concentrations of 20, 40, 60, and 80 nM. The cells were then incubated for an additional 24 hours under the same conditions. Following treatment, 20 µL of MTT reagent was added to each well, and the plates were incubated for 4 hours. The resulting formazan crystals were dissolved in DMSO, and the absorbance was measured at 570 nm using a microplate reader (BioTek Instruments, Winooski, VT, USA). Cell viability (%) was calculated using the following equation [38]:

$$\text{Cell viability (\%)} = \frac{\text{OD of samples at 570 nm}}{\text{OD of control sample at 570 nm}} \times 100$$

Cell apoptosis analysis

Externalization of phosphatidylserine (PS) from the inner to the outer leaflet of the plasma membrane is a hallmark of early apoptosis. This event can be detected by fluorescence staining using Annexin V, which specifically binds to PS on the cell surface [39]. The apoptotic response of MCF-7 cells treated with FPSPFe/siRNA-FAM, FPSPFe/PTX, and FPSPFe/siRNA-FAM/PTX micelles was assessed using flow cytometry. Cells were stained with the Annexin V-Dy634 Apoptosis Detection Kit with Propidium Iodide (PI) (Immunostep, Spain), following the manufacturer's protocol. Data acquisition was performed using a FACSVerse flow cytometer (BD Biosciences, USA), and results were analyzed with FlowJo software (version 10; FlowJo LLC, USA) [40].

siRNA protection assay

To evaluate the nuclease protection capability of FPSPFe/siRNA-FAM/PTX micelles, 8 µL of the nanoparticle suspension (containing 1–6 µg of siRNA) was incubated with either 8 µL of fresh mouse serum or 4 µL of ribonuclease A (RNase A, 20 µg/mL). The mixtures were incubated at 37 °C for up to 24 hours. Following incubation, the residual siRNA was analyzed by 2% agarose gel electrophoresis containing 1% NP-40. Electrophoresis was performed at 80 V, and siRNA bands were visualized to assess integrity and degradation resistance [41].

Transfection assay

To evaluate the cellular uptake of siRNA-FAM, MCF-7 cells were seeded into 24-well plates at a density of 2×10^4 cells/mL in DMEM supplemented with 10% fetal bovine serum (FBS) and incubated at 37 °C in a 5% CO_2 atmosphere for 24 hours. After incubation, FPSPFe/siRNA-FAM micelles containing siRNA-FAM at final concentrations of 100, 200, and 300 µg/mL were added to the wells in triplicate. Naked siRNA (5 µg) was used as a negative control. Following a 7-hour incubation period under the same conditions, the medium was replaced with fresh DMEM containing 10% FBS. Cellular internalization of siRNA-FAM was then assessed using flow cytometry and fluorescence microscopy [37].

Statistical analysis

All quantitative data were obtained from a minimum of three independent replicates. Statistical analyses were performed using SPSS software (version X.X; IBM Corp., Armonk, NY, USA). One-way analysis of variance (ANOVA) was employed to assess differences among groups, followed by Duncan's multiple range test for post hoc comparisons at a significance level of $p < 0.05$. The normality of data distribution was evaluated using the Kolmogorov–Smirnov test. Results are expressed as mean ± standard deviation (SD).

RESULTS

Characteristics of the PLA-spermine-PEG/folic acid copolymer (PSPF)

The chemical structure and thermal stability of the PSPF copolymer were characterized using Fourier-transform infrared (FTIR) spectroscopy and thermogravimetric analysis (TGA).

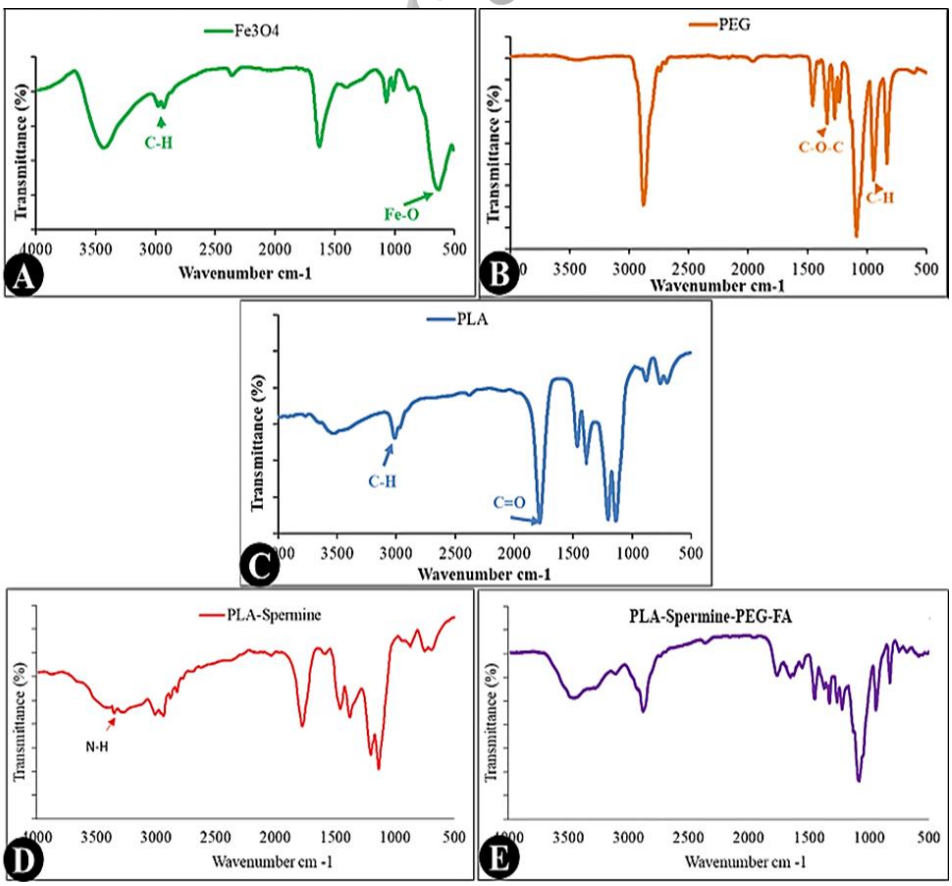

Fig. 1. Images of FTIR spectra of A) Fe_3O_4, B) PEG, C) PLA, D) PLA-spermine, and E) PLA-spermine-PEG/folic acid nanoparticles

FT-IR spectroscopy

FTIR analysis of Fe_3O_4 nanoparticles and the PEG, PLA, and PLA–spermine copolymers revealed characteristic vibrational peaks corresponding to their functional groups. In the spectrum of Fe_3O_4, a prominent peak at 570 cm^{-1} was attributed to Fe–O bond stretching, while a peak at 2950 cm^{-1} was assigned to C–H stretching vibrations (Figure 1A). The PEG spectrum exhibited absorption bands at 980 and 1483 cm^{-1}, corresponding to C–H and C–O–C stretching vibrations, respectively (Figure 1B). For PLA, distinct peaks were observed at 1759 cm^{-1} (C=O stretching), 2955 cm^{-1} (C–H stretching), and 3100 cm^{-1}, consistent with its chemical structure (Figure 1C). The spectrum of spermine showed a peak at 1640 cm^{-1}, corresponding to C=O stretching (amide I), and another at 1560 cm^{-1}, attributed to N–H bending (amide II) (Figure 1D). Additional peaks at 1080 cm^{-1} and 3340 cm^{-1} were assigned to C–O stretching and O–H groups, respectively. Upon conjugation of spermine to PLA, the appearance of a new peak at approximately 1560 cm^{-1} further confirmed the formation of amide bonds (amide II) (Figure 1D). The final PSPF copolymer spectrum (Figure 1E) retained nearly all characteristic peaks of PLA–spermine and PEG–FA, indicating successful chemical incorporation of each component into the copolymer structure.

TGA curves

Figure 2 presents the thermogravimetric analysis (TGA) curves of PLA, PEG–FA, PLA–spermine, PLA–spermine–PEG–FA, and spermine. The results indicate that copolymers containing multiple polymer segments exhibited thermal degradation at higher temperatures compared to individual components. Spermine, for instance, demonstrated a two-step decomposition pattern (Figure 2A). The initial weight loss occurred between 100 °C and 350 °C, likely due to the evaporation of adsorbed water molecules. A second, more significant weight loss was observed between 350 °C and 480 °C, corresponding to the thermal degradation of the spermine backbone. PLA showed a similar two-phase weight loss pattern, consistent with its known thermal profile (Figure 2A). In the case of PEG–FA, multiple stages of thermal decomposition were detected. The first degradation phase initiated at around 100 °C, followed by a second stage that began near 320 °C, and a final, slower decomposition phase that occurred above 370 °C. These observations confirm the multistep thermal behavior of the synthesized polymers and suggest that the copolymer structures exhibit enhanced thermal stability compared to the individual monomers.

As illustrated in Figure 2B, the PSPF copolymer exhibited the most pronounced weight loss stages among the samples, suggesting the presence of multiple constituent components within the copolymer structure. Comparative analysis of TGA curves (Figure 2A vs. 2B) in the temperature range of 380–420 °C revealed that PEG–FA displayed lower thermal resistance than PLA–spermine. Consequently, incorporation of PEG–FA into the PLA–spermine backbone slightly reduced the thermal stability of the resulting PSPF copolymer within this temperature range. This thermal behavior supports the successful chemical integration of PEG–FA, confirming the formation of the intended copolymer.

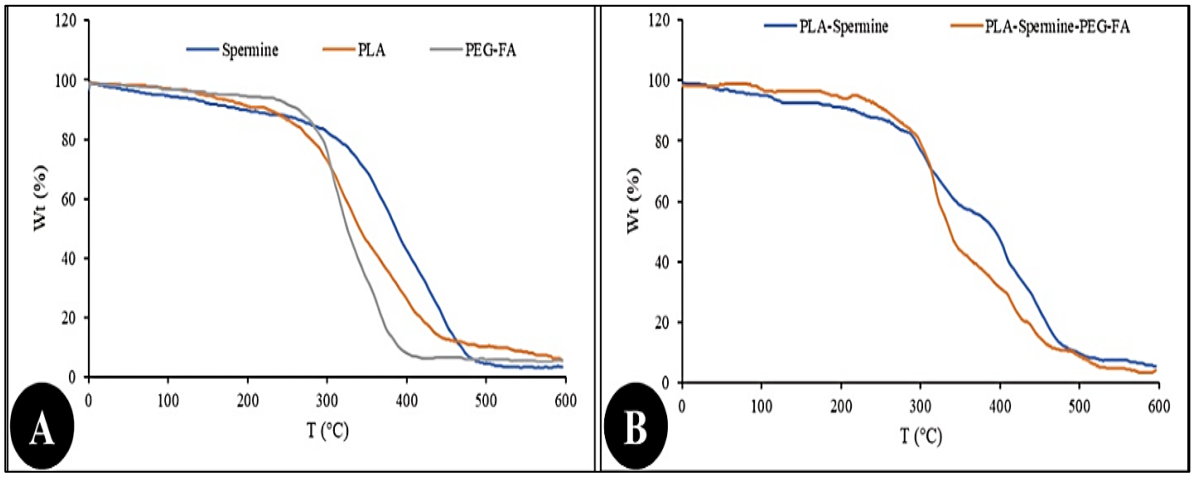

Fig. 2. TGA diagram; A) Spermine, PLA, and PEG-FA polymers, B) PLA-Spermine and PLA-Spermine-PEG-FA (PSPF).

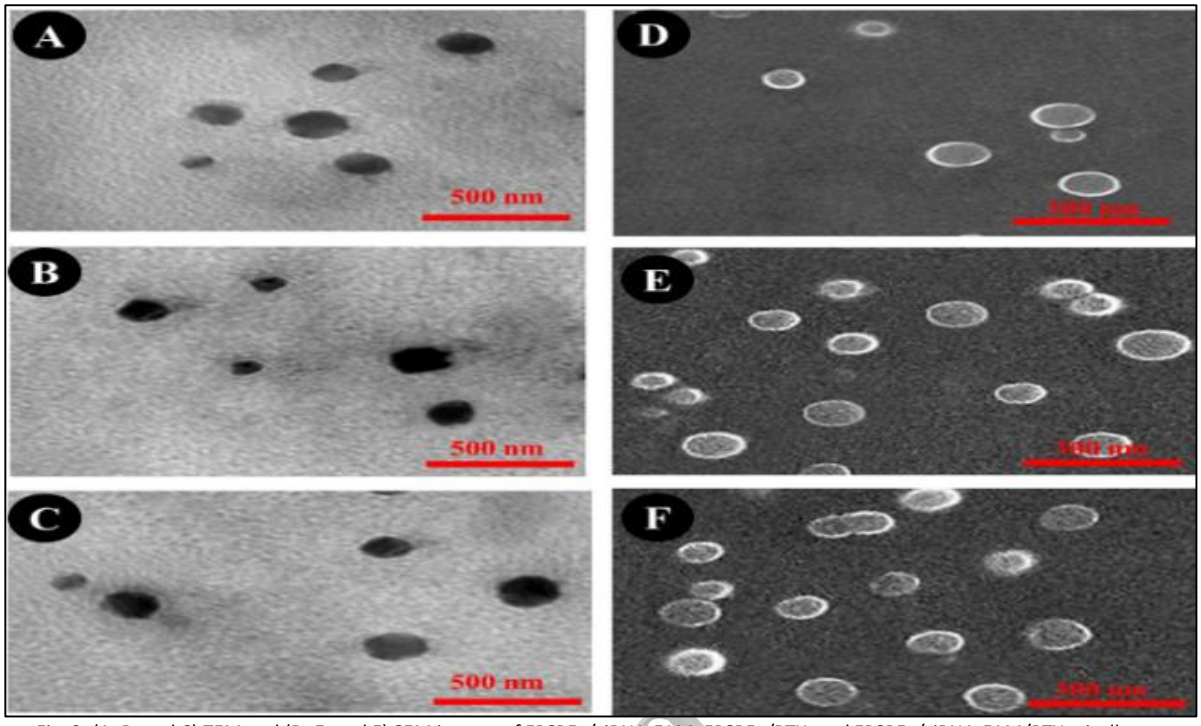

Fig. 3. (A, B, and C) TEM and (D, E, and F) SEM images of FPSPFe/siRNA-FAM, FPSPFe/PTX, and FPSPFe/siRNA-FAM/PTX micelles, respectively.

Table 1. Results of DLS and the zeta potential of the nanoparticles

Nanoparticles	Size	Zeta Potential
FPSPFe	187 ± 8.93 nm	+4.2 mv
FPSPFe/PTX	206 ± 6.10 nm	+3.5 mv
FPSPFe/siRNA-FAM	228 ± 2.11 nm	-3.3 mv
FPSPFe/siRNA-FAM/PTX	259 ± 4.6 nm	+2.2 mv

Morphological characteristics of the micelle nanoparticles

TEM and SEM

Scanning electron microscopy (SEM) and transmission electron microscopy (TEM) analyses confirmed that FPSPFe/siRNA-FAM, FPSPFe/PTX, and FPSPFe/siRNA-FAM/PTX micelles exhibited a uniform, spherical morphology with smooth surfaces. The particle sizes of all three micelle formulations were found to be within the range of 150–200 nm (Figure 3). Moreover, no significant morphological differences were observed among the three formulations, indicating that co-loading of PTX and siRNA-FAM did not affect the overall structural integrity of the micelles.

Zeta potential and nanoparticle size

Dynamic light scattering (DLS) analysis was performed to evaluate the hydrodynamic diameter and zeta potential (surface charge) of FPSPFe nanoparticles and their micellar formulations containing PTX, siRNA-FAM, or both. The average particle sizes of FPSPFe, FPSPFe/PTX, FPSPFe/siRNA-FAM, and FPSPFe/siRNA-FAM/PTX nanoparticles were measured as 187 ± 8.93 nm, 206 ± 6.10 nm, 228 ± 2.11 nm, and 259 ± 6.4 nm, respectively (Table 1; Figure 4A–D). While the observed size differences were not statistically significant, a gradual increase in nanoparticle diameter was noted upon the encapsulation of PTX, siRNA-FAM, and their combination. These results suggest that the incorporation of therapeutic agents has a slight influence on the overall size of the micelles, without compromising their nanoscale range.

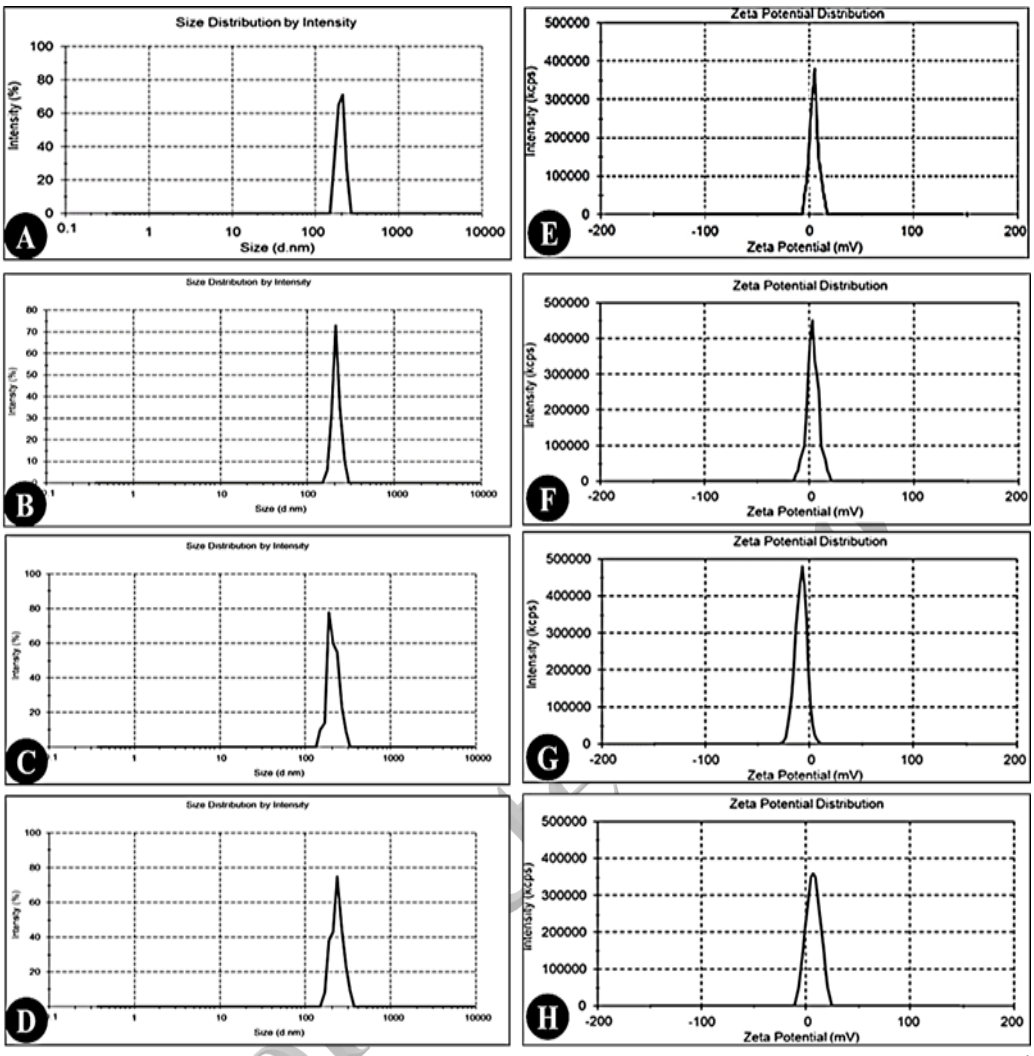

Fig. 4. Size (A, B, C, and D) and zeta potential (E, F, G, and H) of synthesized nanoparticles; (A and E) FPSPFe, (B and F) FPSPFe/PTX, (C and G) FPSPFe/siRNA-FAM, and (D and H) FPSPFe/siRNA-FAM/PTX micellar nanoparticles.

Zeta potential is a critical parameter in nanoscience and biology, used to characterize the surface properties of nanoparticles. It specifically refers to the electrical charge at the interface of nanoparticles suspended in a solution and is influenced by various factors, including material type, particle size, pH, and electrolyte concentration [42]. Based on the results of this study, the zeta potentials of the FPSPFe copolymer nanoparticles and the micellar formulations—FPSPFe/PTX, FPSPFe/siRNA-FAM, and FPSPFe/siRNA-FAM/PTX—were measured as +4.2, +3.5, -3.3, and +2.2 mV, respectively (Table 1 and Figure 4E–H). The positive zeta potential of FPSPFe copolymer nanoparticles was attributed to the presence of cationic polymers. However, the incorporation of folic acid and Fe_3O_4 nanoparticles reduced the overall surface charge. Furthermore, the incorporation of PTX, siRNA-FAM, or their combination into the micellar nanoparticles led to a reduction in zeta potential. Notably, the addition of siRNA-FAM resulted in a negative surface charge, which can be attributed to the presence of negatively charged functional groups on the siRNA molecules. Interestingly, co-loading PTX with siRNA-FAM partially restored the surface potential, increasing its value. Based on the observed size and zeta potential profiles, the synthesized nanoparticles demonstrate favorable characteristics for the efficient delivery of both therapeutic agents and genetic material.

Magnetic Properties of Micellar Nanoparticles

Due to their strong magnetic characteristics, Fe_3O_4 nanoparticles have significant applications in targeted drug delivery and imaging systems [19]. The saturation magnetization of the studied samples ranged from 18.4 to 36.8 emu/g (electromagnetic units per gram). However, coating Fe_3O_4 nanoparticles with FPSP micelles resulted in

a noticeable reduction in their magnetic properties. These findings are consistent with previous studies. Specifically, the saturation magnetization values of FPSPFe/siRNA-FAM, FPSPFe/PTX, and FPSPFe/siRNA-FAM/PTX micelles were 18.4, 20.3, and 19.6 emu/g, respectively, lower than those of bare Fe_3O_4 nanoparticles (Figure 5). As with most magnetic nanoparticles, encapsulation with nonmagnetic compounds leads to a decline in overall magnetic response.

siRNA loading and release patterns from the FPSPFe copolymer

The analysis of loading efficiency revealed that siRNA-FAM exhibited a higher loading percentage than PTX in both FPSPFe copolymers and FPSPFe-based micelles. Moreover, the encapsulation efficiency of siRNA-FAM was enhanced when co-delivered with PTX in FPSPFe/PTX micelles, compared to encapsulation using the FPSPFe copolymer alone. Specifically, the loading efficiency of siRNA-FAM decreased from 85% to 75% when co-encapsulated with PTX. Conversely, the encapsulation efficiency of PTX increased from 49% to 60% when delivered alongside siRNA-FAM in FPSPFe-based micelles (Figure 6).

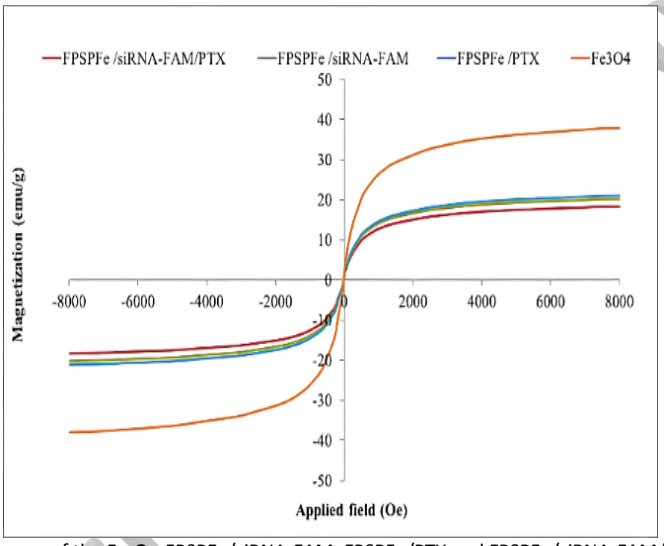

Fig. 5. VSM images of the Fe_3O_4, FPSPFe/siRNA-FAM, FPSPFe/PTX and FPSPFe/siRNA-FAM/PTX micelles.

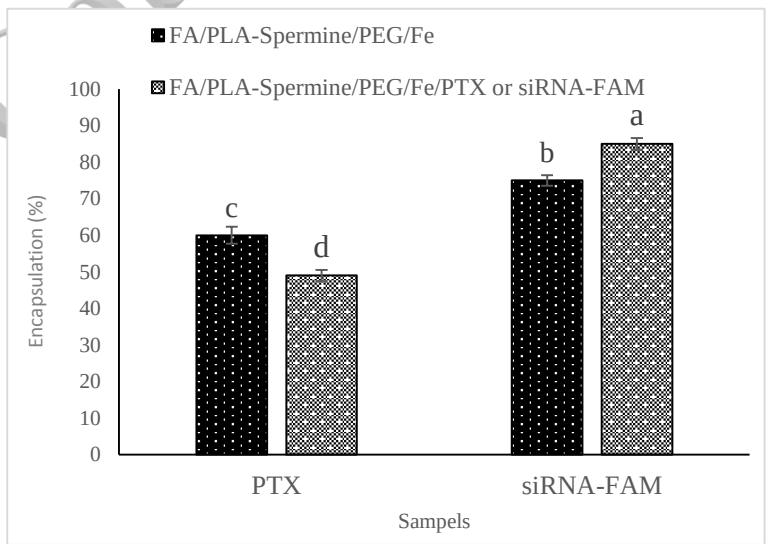

Fig. 6. Comparison chart of the average encapsulation efficiency of siRNA-FAM and PTX in FPSPFe and FPSPFe/siRNA-FAM or PTX copolymers.
*Different letters indicate significant differences (at the 5% probability level) among the treatments at each of the studied time points. Specify statistical test (ANOVA, Duncan)

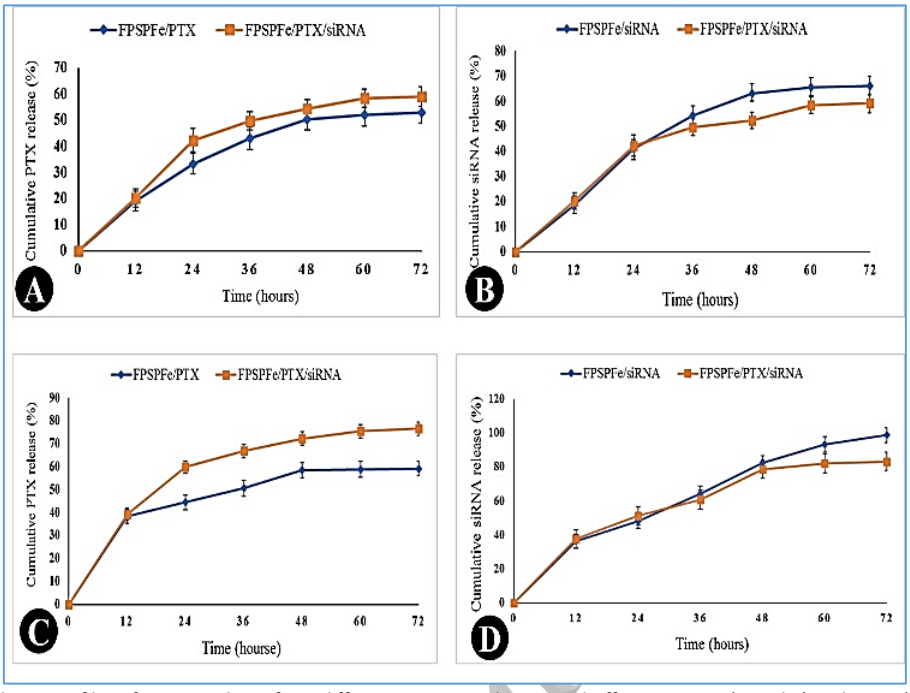

Fig. 7. Release profiles of siRNA and PTX from different nanoparticles in PBS buffer at pH=7.4 (A and B) and pH=6 (C and D).

*Different letters indicate significant ifferences (at the 5% probability level) among the treatments at each of the studied time points. Specify statistical test (ANOVA, Duncan)

To evaluate the drug half-life and release profile of the micellar nanoparticles in both systemic circulation and tumor environments, *in vitro* release studies were conducted under acidic (pH 6.0) and physiological (pH 7.5) conditions. A biphasic release pattern was observed for both PTX and siRNA (Figure 7). The initial phase involved a rapid release of a substantial portion of the encapsulated agents, followed by a sustained and slower release over an extended period. This release behavior aligns with previous reports suggesting that during the encapsulation process, therapeutic agents can localize within different micellar compartments, contributing to staged release dynamics. Due to the greater exposure of the micelle surface layer to the polar buffer environment, this layer undergoes faster degradation, resulting in the rapid release of surface-encapsulated drugs. In contrast, the inner layers or core of the micelle degrade more slowly due to the gradual infiltration of water, resulting in sustained drug release. Drug release studies revealed that both PTX and siRNA exhibited significantly higher release rates in acidic phosphate-buffered saline (pH 6.0) compared to neutral conditions (pH 7.5). This observation is consistent with prior findings indicating that the extracellular pH of most tumor tissues is approximately 6.0, while that of normal tissues is closer to 7.0. Therefore, the enhanced release of therapeutics under acidic conditions suggests that these nanoparticles may improve drug delivery to tumor sites while minimizing off-target effects on healthy tissues (Figure 7).

In vitro cytotoxicity assay

The half-maximal inhibitory concentration (IC_{50}) is a widely used parameter for assessing the impact of drugs or chemical compounds on cellular and organismal biological activity [43]. In the context of cancer therapy, IC_{50} represents the concentration of a compound required to inhibit the viability of a specific cancer cell type by 50%, making it a critical metric for evaluating the efficacy of anticancer agents [44]. In this study, FPSPFe and FPSPFe/siRNA-FAM nanoparticles demonstrated low cytotoxicity, with IC_{50} values of 71.24 and 43.17 µg/mL, respectively (Figures 8 and 9). However, a marked increase in cytotoxicity was observed following PTX encapsulation, resulting in reduced IC_{50} values of 29.83 and 34.88 µg/mL, respectively. These findings suggest that incorporation of PTX significantly enhances the cytotoxic potential of the nanoparticles (Figure 9). Free PTX was included as a positive control for comparison.

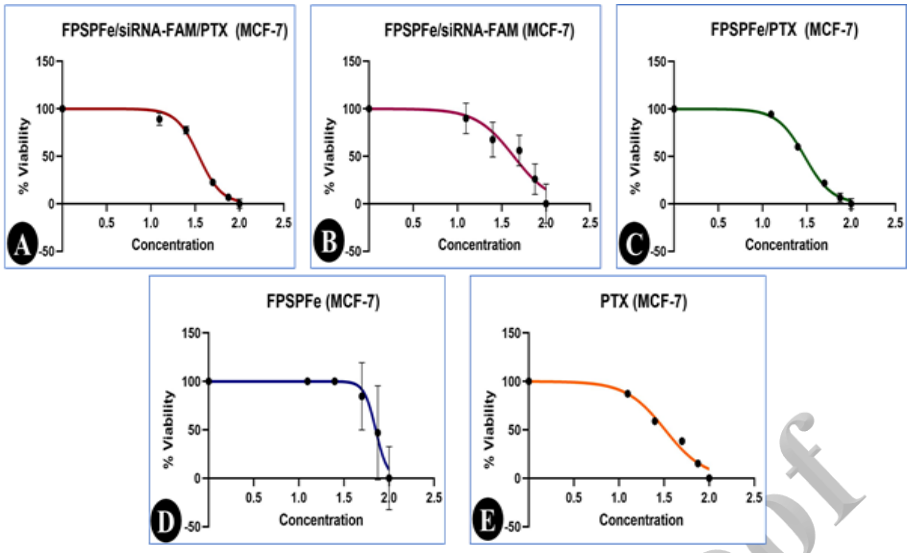

Fig. 8.Comparison of the average effects of A) FPSPFe, B) FPSPFe/siRNA-FAM, C) FPSPFe/PTX, D) FPSPFe/siRNA-FAM/PTX, and E) PTX micelles on the viability of the MCF-7 cell line.

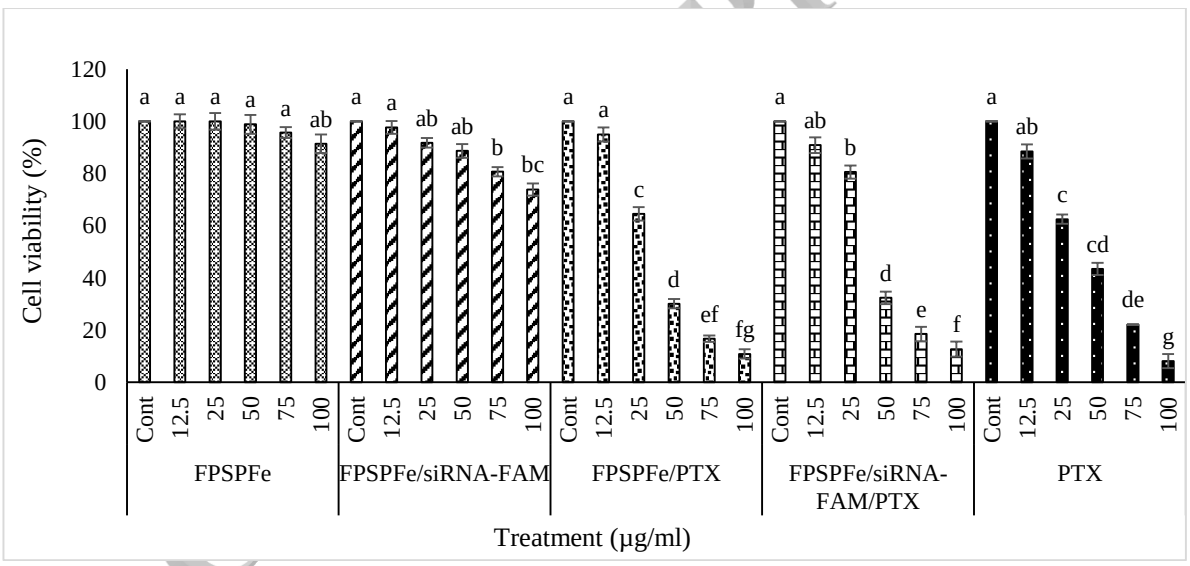

Fig. 9. Cytotoxicity of different nanoparticles at different concentrations to the MCF-7 cell line.
*Different letters indicate significant differences (at the 5% probability level) among the treatments at each of the studied time points. Specify statistical test (ANOVA, Duncan)

Cellular apoptosis

Apoptosis, or programmed cell death, is a tightly regulated process by which cells are eliminated in a controlled manner without triggering inflammation or harming surrounding tissues. This mechanism is essential for maintaining tissue homeostasis and eliminating damaged or unnecessary cells. Targeted micelles have shown potential in promoting apoptosis selectively in cancer cells while minimizing off-target effects. In the present study, following the determination of IC_{50} values, the pro-apoptotic effects of the formulations were investigated. The results revealed that treatment with free PTX led to the highest percentage of necrotic cells (29.11%), indicating substantial cytotoxicity (Figure 10 and Figure 11E). Furthermore, consistent with previous reports, the elevated percentage of necrotic cells observed in the control group may be attributed to the rapid proliferation of the MCF-7 cell line and competition for nutrients under *in vitro* conditions (Figures 10 and 11A). In contrast, the low percentage of necrotic cells in the FPSPFe/siRNA-FAM-treated group suggests minimal off-target effects and good biocompatibility of both the micellar carrier and siRNA-FAM (Figure 10 and Figure 11B). Notably, the highest percentages of cells in the early and late apoptotic phases—15.76% and 11.23%,

respectively—were observed following treatment with FPSPFe/PTX (Figures 10 and 11C). These findings support the role of the FPSPFe nanoparticle system in enhancing programmed cell death and improving the therapeutic efficacy of PTX. As illustrated in Figure 10, treatment with free PTX resulted in a high percentage of necrotic cells, while the proportions of cells undergoing early and late apoptosis were comparatively low. In contrast, encapsulation of PTX within FPSPFe nanoparticles significantly reduced necrosis and promoted apoptosis, as evidenced by increased percentages of cells in both apoptotic phases. These observations suggest that FPSPFe nanoparticles enhance the apoptotic response while mitigating nonspecific cytotoxic effects associated with free PTX. Due to their unique physicochemical properties, nanoparticles can exert diverse effects on the apoptotic pathway, either enhancing or inhibiting it, depending on their size, shape, surface characteristics, and composition.

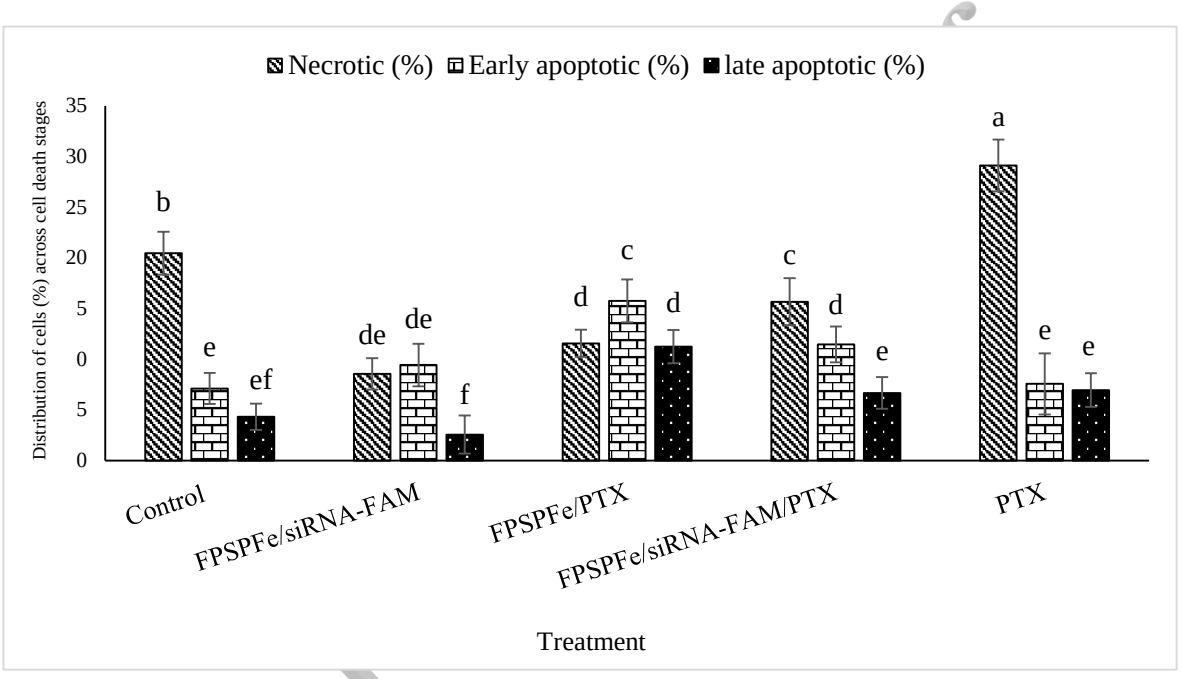

Fig. 10. Percentages of MCF-7 cells in the necrotic, pre- and post-apoptosis stages affected by the calculated IC_{50} concentrations of FPSPFe/siRNA-FAM, FPSPFe/PTX, FPSPFe/siRNA-FAM/PTX, PTX nanoparticles and the control treatment.
*Different letters indicate significant differences (at the 5% probability level) among the treatments at each of the studied time points. Specify statistical test (ANOVA, Duncan)

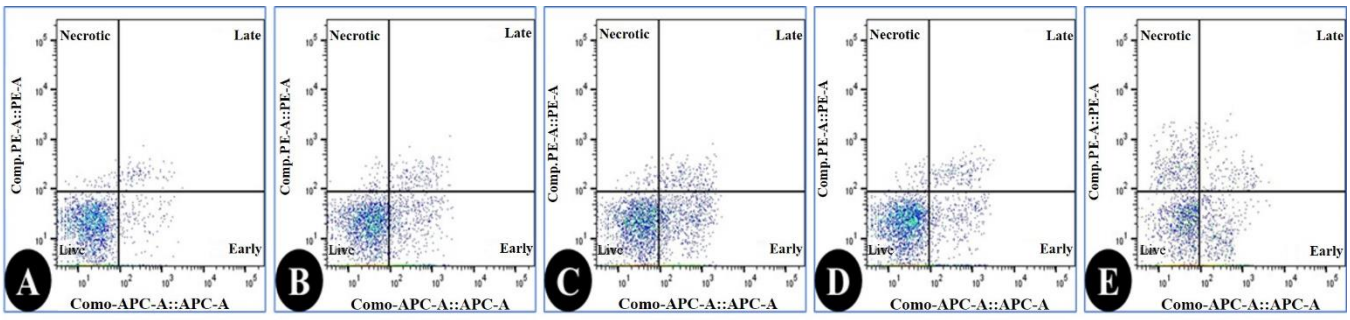

Fig. 11. Schematic flow cytometry image of MCF-7 cells in the necrotic, pre- and post-apoptosis stages under the influence of the calculated IC_{50} concentrations of A) the control treatment, B) FPSPFe/siRNA-FAM, C) FPSPFe/PTX, D) FPSPFe/siRNA-FAM/PTX, and E) PTX.

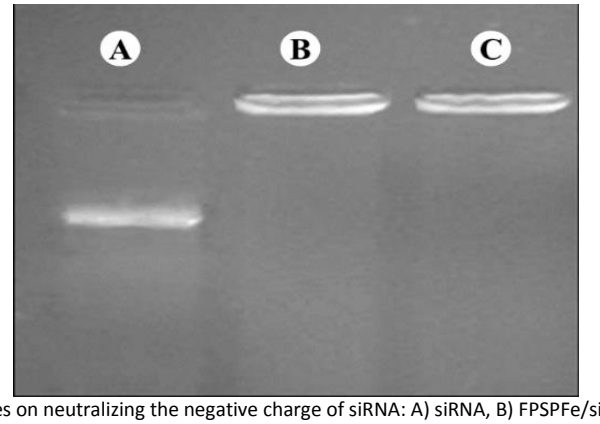

Fig. 12. Effect of FPSPFe micelles on neutralizing the negative charge of siRNA: A) siRNA, B) FPSPFe/siRNA-FAM, and FPSPFe/siRNA-FAM/PTX.

siRNA protection

The ability of nanoparticles to neutralize the negative charge of siRNA is critical for its effective cellular uptake and delivery to cancer cells [26]. To assess this property, agarose gel electrophoresis was performed to evaluate the mobility of siRNA in the presence of FPSPFe nanoparticles. In this system, spermine served as a cationic agent within the copolymer structure, facilitating interaction with the negatively charged siRNA. The results showed that siRNA migration was inhibited entirely, indicating successful complexation with FPSPFe nanoparticles (Figure 12). This effect is likely due to electrostatic interactions between the amine groups of spermine and the phosphate backbone of the siRNA. Notably, the co-loading of PTX did not interfere with the ability of FPSPFe nanoparticles to neutralize the negative charge of siRNA-FAM (Figure 12).

Cellular transfection assay

The cellular uptake and delivery efficiency of siRNA-FAM by FPSPFe micelles were evaluated in MCF-7 cells using flow cytometry and fluorescence microscopy (Figures 13–15). The results demonstrated successful intracellular delivery and release of siRNA-FAM. Furthermore, the transfection efficiency was found to be concentration-dependent, with transfection rates of 42%, 51%, and 58% observed at nanoparticle concentrations of 100, 200, and 300 µg/mL, respectively (Figure 15).

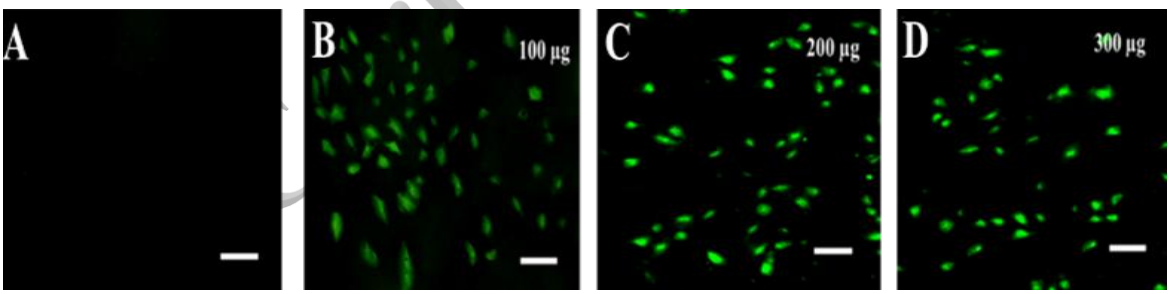

Fig. 13. Fluorescence microscopy images of A) control cells and B, C and D) cells treated with 100, 200, and 300 µg of FPSPFe/siRNA-FAM micelles, respectively.

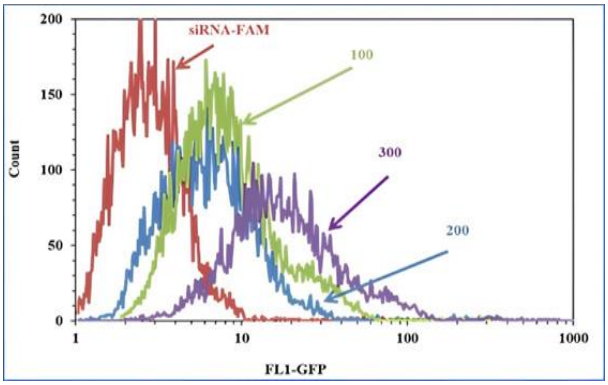

Fig. 14. Flow cytometry images of control cells treated with siRNA-FAM and cells treated with 100, 200, and 300 µg of FPSPFe/siRNA-FAM micelles.

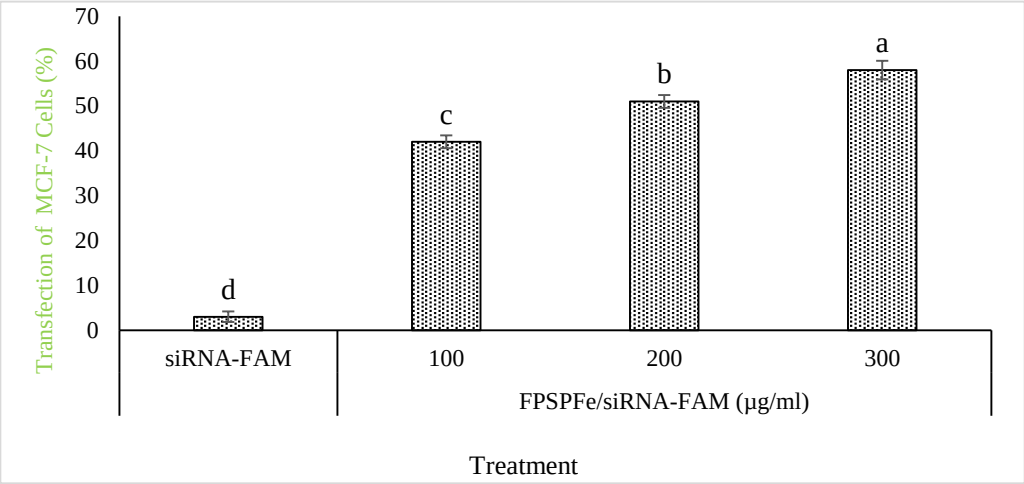

Fig. 15. siRNA transfection rate into MCF-7 cells by siRNA-FAM and 100, 200, and 300 µg of FPSPFe/siRNA-FAM micelles after 24 h
*Different letters indicate significant differences (at the 5% probability level) among the treatments at each of the studied time points. Specify statistical test (ANOVA, Duncan)

DISCUSSION

Cancer remains one of the most significant global health challenges, with breast cancer representing one of the most prevalent and lethal malignancies among women [1]. Although advances in diagnosis and treatment have improved patient outcomes, conventional therapies such as chemotherapy and radiotherapy often lead to severe systemic side effects due to their lack of selectivity. In recent years, nanotechnology has emerged as a promising approach for cancer therapy, offering the potential for targeted drug delivery through the use of intelligent nanocarriers [8]. Among these, polymeric nanoparticles—particularly those based on PLA-PEG copolymers—have demonstrated excellent biocompatibility and can be functionalized with targeting ligands such as folic acid (FA) to enhance specificity. Furthermore, the incorporation of Fe_3O_4 nanoparticles enables magnetic targeting and real-time imaging, facilitating precise accumulation at tumor sites. These innovations collectively improve therapeutic efficacy while reducing off-target toxicity.

A promising and innovative strategy in cancer therapy involves the co-delivery of siRNA alongside chemotherapeutic agents such as PTX using advanced nanocarrier systems. siRNAs possess strong potential to silence oncogenes; however, their clinical translation is limited by inherent instability and inefficient cellular internalization [30]. Polymeric nanoparticles offer a viable solution by shielding siRNA from enzymatic degradation and enhancing its intracellular delivery. When co-delivered with PTX, the system exerts a synergistic therapeutic effect: PTX interferes with microtubule dynamics, arresting cell division, while siRNA downregulates anti-apoptotic genes, such as Bcl-2, thereby overcoming chemoresistance. The nanocarrier design further incorporates spermine to promote endosomal escape and employs a pH-responsive release mechanism tailored to the acidic tumor microenvironment [31]. This multifunctional platform not only amplifies treatment efficacy but also underscores the transformative potential of nanomedicine in enabling precise, combinatorial cancer therapies.

In this study, PSPF copolymer nanoparticles were developed in combination with Fe_3O_4 magnetic nanoparticles for the co-delivery of siRNA and the chemotherapeutic agent PTX to MCF-7 breast cancer cells. Characterization of the nanoparticles' physicochemical properties using Fourier-transform infrared spectroscopy (FTIR) was essential for confirming their structural integrity and chemical composition. The FTIR spectra validated the presence of the anticipated functional groups within the nanoparticle architecture (Figure 1). Specifically, the Fe–O stretching vibration of Fe_3O_4 was observed at 570 cm^{-1}. Peaks at 980 cm^{-1} and 1483 cm^{-1} corresponded to the C–O–C and C–H stretching vibrations of PEG, respectively, in agreement with previous reports [45], thereby confirming the successful integration of Fe_3O_4 into the PEG-based copolymer matrix.

Thermogravimetric analysis (TGA) is a crucial technique for evaluating the physicochemical properties of nanoparticles, offering insights into their thermal stability, organic and inorganic composition, and degradation behavior. TGA analysis of PSPF nanoparticles revealed a two-step thermal degradation profile for both spermine and PLA components. Additionally, the PEG–FA conjugate exhibited multiple weight loss events, suggesting complex thermal decomposition associated with the linkage between PEG and folic acid (Figure 2).

Nanoparticle shape and morphology are crucial parameters that influence the efficiency of targeted gene delivery systems. Transmission electron microscopy (TEM) and scanning electron microscopy (SEM) images obtained in this study (Figure 3D–F) confirmed that FPSPFe/siRNA-FAM, FPSPFe/PTX, and FPSPFe/siRNA-FAM/PTX micelles exhibited a uniform spherical morphology. Previous studies have shown that spherical nanoparticles offer superior cellular uptake and are more effective in delivering therapeutic agents and genetic material [46].

In targeted gene delivery, nanoparticle size and surface charge are critical determinants that significantly influence the efficacy and transfection efficiency of gene-based therapies. As demonstrated in this study (Table 1; Figures 4A–D), the measured sizes of FPSPFe, FPSPFe/PTX, FPSPFe/siRNA-FAM, and FPSPFe/siRNA-FAM/PTX micelles fall within the optimal range for efficient gene delivery into eukaryotic cells [47].

Effective optimization of nanocarriers for gene and drug delivery necessitates a comprehensive understanding of how environmental and chemical factors modulate their performance. Among these, pH is a critical parameter, as the acidic microenvironment of tumor tissues (pH 4.5–6.5) contrasts with that of healthy tissues (pH 7.4), enabling the design of pH-responsive delivery systems. Experimental analysis of FPSPFe nanoparticles demonstrated that, due to electrostatic interactions, the loading efficiency of siRNA (85%) exceeded that of PTX (49%). However, simultaneous co-loading resulted in a slight reduction in siRNA loading (to 75%) and a notable increase in PTX loading (to 60%), indicative of competitive binding dynamics. Drug release exhibited a biphasic profile, characterized by an initial burst release from the nanoparticle surface followed by a sustained release from the core. Importantly, release rates under acidic conditions (pH 6.0) were 1.5- to 2-fold higher than those at neutral pH (7.4). These findings underscore the promise of pH-responsive nanocarriers in enabling precise, synergistic cancer therapies through controlled co-delivery of genetic and chemotherapeutic agents [48].

In contrast, the results of this study demonstrated that FPSPFe and FPSPFe/siRNA-FAM micelles exhibited significantly lower cytotoxicity compared to PTX-containing formulations, namely FPSPFe/PTX and FPSPFe/siRNA-FAM/PTX (Figures 8 and 9). The increased cytotoxicity in the latter groups can be attributed to the well-established mechanism of PTX, which inhibits cell division by disrupting microtubule dynamics and preventing the formation of the mitotic spindle. This interference ultimately halts the proliferation of cancer cells [5].

Compared to conventional lipid- and polymer-based nanoparticle systems, the Fe_3O_4-loaded micellar nanoparticles exhibited favorable biocompatibility, as evidenced by their toxicity profiles (Figures 8 and 9). While lipid-based carriers such as liposomes are generally biocompatible, they may induce toxicity at high concentrations due to lipid degradation. Similarly, polymer-based nanoparticles—particularly cationic variants—are known to provoke inflammatory responses. In contrast, the Fe_3O_4-micelle platform demonstrated reduced cytotoxicity by limiting direct exposure to iron oxide, suppressing the generation of reactive oxygen species (ROS), and offering a balanced combination of lipid safety and polymer stability. However, potential long-term risks related to iron accumulation warrant further investigation. Overall, this hybrid system represents a promising candidate for applications involving high or repeated dosing regimens [49].

The higher cytotoxicity observed in PTX-containing micelles compared to empty micelles is primarily attributed to the rapid initial release of PTX and its inherent cytotoxicity (Figures 8 and 9). This burst release likely causes localized drug accumulation in the culture medium, leading to cellular stress and functional disruption [50]. Notably, the co-encapsulation of siRNA and PTX within a single, targeted nanocarrier enables synchronized intracellular delivery, as supported by enhanced cytotoxic effects in MCF-7 cells (MTT assay) and efficient cellular uptake (flow cytometry analysis). Moreover, the accelerated release of therapeutic agents under acidic conditions highlights the system's responsiveness to tumor-specific microenvironments, enhancing therapeutic synergy while minimizing unintended effects on healthy tissues.

Consequently, the typically negative charges on both the gene sequence and the cell membrane are neutralized to some extent, reducing electrostatic repulsion and facilitating cellular uptake. Moreover, electrostatic interactions between siRNA and the FPSPFe nanoparticles promote the condensation of siRNA into a stable, compact spherical structure. This not only enhances gene transfer efficiency but also protects siRNA from degradation by nucleases and other destabilizing factors in the circulatory system. As previously reported, enzymatic digestion of siRNA requires access to specific binding sites by restriction enzymes [51]. In this study, the interaction between FPSPFe and siRNA effectively shielded the siRNA from enzymatic cleavage (Figure 12). Consistent with prior findings, the physical compression and reduced surface exposure of siRNA within the nanoparticle complex appear to limit enzyme accessibility, thereby preventing the degradation of siRNA.

CONCLUSION

This study aimed to develop a dual-functional micellar nanocarrier capable of simultaneously delivering siRNA and paclitaxel (PTX) to cancer cells. The synthesized FPSPFe nanoparticles demonstrated high gene transfer efficiency with minimal toxicity and adverse effects. Drug release analysis under physiological (pH 7.4) and acidic (pH 6.0) conditions revealed a pH-responsive release profile, characterized by rapid release in acidic environments and sustained release under neutral conditions. This behavior is particularly advantageous for cancer therapy, as it facilitates increased drug release within the acidic tumor microenvironment while minimizing off-target exposure in healthy tissues. Overall, the FPSPFe nanocarrier system presents a promising platform for synergistic and targeted cancer treatment through the co-delivery of chemotherapeutic and gene-silencing agents. Consequently, the FPSPFe nanoparticles not only enhance selective cytotoxicity toward cancer cells but also minimize adverse effects on healthy tissues. Our findings confirm that siRNA molecules effectively interact with the micellar structure, resulting in partial neutralization of their negative charge. This interaction plays a critical role in improving endosomal escape and facilitating intracellular delivery. Furthermore, the successful co-delivery of PTX and siRNA by the FPSPFe system may contribute to overcoming drug resistance mechanisms, highlighting its potential for advanced combination therapies in cancer treatment.

SUGGESTIONS FOR FUTURE STUDIES

1) Pharmacokinetics and Biodistribution

- Plasma half-life, assessment of clearance and tumor accumulation in orthotopic breast cancer mouse models via fluorescence (siRNA-FAM) and high-performance liquid chromatography (HPLC) (PTX)

- Dual labelling (e.g., Cy5.5 for nanoparticles + ^{3}H-PTX) can distinguish the biodistribution of the carrier from that of the free drug.

2) Efficacy and Safety

- Tumor growth inhibition and survival studies, PSPF/siRNA/PTX with single-drug treatments and comparisons with controls

- Toxicity assessment via blood/biochemical markers and significant organ histopathology

3) Mechanistic validation

- *Ex vivo* tumor tissue analysis, confirmation of siRNA-mediated gene silencing (qPCR/Western blot), and PTX-induced apoptosis (TUNEL assay).

ACKNOWLEDGEMENTS

We would like to express my heartfelt gratitude to everyone who contributed to the completion of this article.

FUNDING

The authors did not receive support from any organization for the submitted work.

CONFLICT OF INTEREST

The authors declare that there are no conflicts of interest.

AUTHOR CONTRIBUTIONS

SM conducted the experiments, analysed the data, and wrote the original draft. HY and SM conceived and designed the research, administered and supervised the project, and HY reviewed and edited the manuscript. All the authors read and approved the manuscript.

DATA AVAILABILITY

The authors declare that the data supporting the findings of this study are available within the paper and its Supplementary Information files. Should any raw data files be required in an alternative format, they are available from the corresponding author upon reasonable request.

REFERENCES

1. Arnold M, Morgan E, Rumgay H, Mafra A, Singh D, Laversanne M, Vignat J, Gralow JR, Cardoso F, Siesling S. Current and future burden of breast cancer: Global statistics for 2020 and 2040. Breast. 2022;66:15-23.

2. Organization WH. Breast Cancer 2024 [Available from:https://www.who.int/news-room/fact-sheets/detail/breast-cancer.
3. Alrushaid N, Khan FA, Al-Suhaimi EA, Elaissari A. Nanotechnology in cancer diagnosis and treatment. Pharmaceutics. 2023;15(3):1025.
4. Kaloni D, Diepstraten ST, Strasser A, Kelly GL. BCL-2 protein family: attractive targets for cancer therapy. Apoptosis. 2023;28(1):20-38.
5. Raj S, Khurana S, Choudhari R, Kesari KK, Kamal MA, Garg N, Ruokolainen J, Das BC, Kumar D, editors. Specific targeting cancer cells with nanoparticles and drug delivery in cancer therapy. Seminars in cancer biology; 2021: Elsevier.
6. Bourang S, Jahanbakhsh Godehkahriz S, Noruzpour M, Asghari Zakaria R, Granados-Principal S. Anticancer properties of copolymer nanoparticles loaded with *Foeniculum vulgare* derivatives in Hs578T and SUM159 cancer cell lines. Cancer Nanotechnol. 2025;16(1):1-28.
7. Wang J, Zhuang S. Chitosan-based materials: Preparation, modification and application. J Clean Prod. 2022;355:131825.
8. Bourang S, Noruzpour M, Jahanbakhsh Godekahriz S, Ebrahimi HAC, Amani A, Asghari Zakaria R, Yaghoubi H. Application of nanoparticles in breast cancer treatment: a systematic review. Naunyn Schmiedebergs Arch Pharmacol. 2024:1-47.
9. Ucal S. Polyamine analogues as anticancer agents: Itä-Suomen yliopisto; 2017.
10. Sagar NA, Tarafdar S, Agarwal S, Tarafdar A, Sharma S. Polyamines: functions, metabolism, and role in human disease management. Med Sci. 2021;9(2):44.
11. Ghasemi S, Owrang M, Javaheri F, Farjadian F. Spermine modified PNIPAAm nano-hydrogel serving as thermo-responsive system for delivery of cisplatin. Macromol Res. 2022;30(5):314-324.
12. Abri N, Vasheghani-Farahani E, Shaki H, Ganji F, Jafarzadeh-Holahg S. Magnetic dextran-spermine nanoparticles as pH-sensitive carriers for antibiotic delivery. J Nanopart Res. 2024;26(4):73.
13. Mohajeri S, Yaghoubi H, Bourang S, Noruzpour M. Multifunctional magnetic nanocapsules for dual delivery of siRNA and chemotherapy to MCF-7 cells (Breast cancer cells). Naunyn Schmiedebergs Arch Pharmacol. 2025; 27:1-23.
14. Jin Y, Wang X, Kromer AP, Müller JT, Zimmermann C, Xu Z, Hartschuh A, Adams F, Merkel OM. Role of Hydrophobic Modification in Spermine-Based Poly (β-amino ester) s for siRNA Delivery and Their Spray-Dried Powders for Inhalation and Improved Storage. Biomacromolecules. 2024.
15. Scott AM, Zhang Z, Jia L, Li K, Zhang Q, Dexheimer T, Ellsworth E, Ren J, Chung-Davidson Y-W, Zu Y. Spermine in semen of male sea lamprey acts as a sex pheromone. PLoS Biol. 2019;17(7):e3000332.
16. Zou W, Liu C, Chen Z, Zhang N. Preparation and characterization of cationic PLA-PEG nanoparticles for delivery of plasmid DNA. Nanoscale Res Lett. 2009;4:982-92.
17. Mundel R, Thakur T, Chatterjee M. Emerging uses of PLA–PEG copolymer in cancer drug delivery. 3 Biotech. 2022;12(2):41.
18. Chung S, Sugimoto Y, Huang J, Zhang M. Iron oxide nanoparticles decorated with functional peptides for a targeted siRNA delivery to glioma cells. ACS Appl Mater Interfaces. 2022;15(1):106-119.
19. Noruzpuor M, Asghari Zakaria R, Zare N, Ebrahimi HA, Parsa H, Bourang S. Green synthesis of metal nanoparticles using aqueous extract of *Moringa oleifera* L. and investigating their antioxidant and antibacterial properties. Appl Chem Today. 2024;19(71):283-302.
20. Bourang S, Asadian S, Noruzpour M, Mansuryar A, Azizi S, Ebrahimi HA, Amani Hooshyar V. PLA-HA/Fe_3O_4 magnetic nanoparticles loaded with curcumin: physicochemical characterization and toxicity evaluation in HCT116 colorectal cancer cells. Discov appl sci. 2024;6(4):186.
21. Noruzpour M, Zakaria RA, Zare N, Bourang S, Ebrahimi HA, Granados-Principal S. Delivery of Moringa oleifera Extract via PLA-PEG-FA/Chitosan-PLA NPs into Breast Cancer Cell Lines. Bio Nano Science. 2025;15(2):287.
22. Asghari Zakaria R, Zare N, Ebrahimi HA, Parsa H, Bourang S. Investigating the anticancer properties of the essential oil and aqueous extract of *Moringa oleifera* and its biosynthesized metal nanoparticles on MCF-7 and BT-549 cell lines. IJBD. 2024;17(1):59-83.
23. Gangopadhyay S, Nikam RR, Gore KR. Folate receptor-mediated siRNA delivery: recent developments and future directions for RNAi therapeutics. Nucleic Acid Ther. 2021;31(4):245-70.
24. Salim L, Desaulniers J-P. To conjugate or to package? A look at targeted siRNA delivery through folate receptors. Nucleic Acid Ther. 2021;31(1):21-38.
25. Narayanan KB, Bhaskar R, Han SS. Recent advances in the biomedical applications of functionalized nanogels. Pharmaceutics. 2022;14(12):2832.
26. Cavallaro G, Sardo C, Craparo EF, Porsio B, Giammona G. Polymeric nanoparticles for siRNA delivery: Production and applications. Int J Pharm. 2017;525(2):313-33.
27. Dastgerdi NK, Dastgerdi NK, Bayraktutan H, Costabile G, Atyabi F, Dinarvand R, Longobardi G, Alexander C, Conte C. Enhancing siRNA cancer therapy: Multifaceted strategies with lipid and polymer-based carrier systems. Int J Pharm. 2024:124545.
28. Yaghoubi H, Eskanlou H, Danandeh Baghrabad M, Farazi N, Nedaee Shakarab B. Preparation and evaluation of anti-cancer effects of targeted polymer nano particles containing paclitaxel and siRNA in MCF-7 breast cancer cell line. Cellular and Molecular Research (Iranian Journal of Biology). 2023.
29. Amani A, Dustparast M, Noruzpour M, Zakaria RA, Ebrahimi HA. Design and invitro characterization of green synthesized magnetic nanoparticles conjugated with multitargeted poly lactic acid copolymers for co-delivery of siRNA and paclitaxel. Eur J Pharm Sci. 2021;167:106007.

30. Noruzpour M, Zakaria RA, Zare N, Bourang S, Ebrahimi HA, Granados-Principal S. Delivery of *Moringa oleifera* extract via PLA-PEG-FA/chitosan-PLA NPs into breast cancer cell lines. Bionanoscience. 2025;15(2):287.
31. Haddad R, Alrabadi N, Altaani B, Li T. Paclitaxel drug delivery systems: Focus on nanocrystals' surface modifications. Polymers. 2022;14(4):658.
32. Kumar K, Rani V, Mishra M, Chawla R. New paradigm in combination therapy of siRNA with chemotherapeutic drugs for effective cancer therapy. Curr Res Pharmacol Drug Discov. 2022;3:100103.
33. Xue R, Pan Y, Xia L, Li J. Non-viral vectors combined delivery of siRNA and anti-cancer drugs to reverse tumor multidrug resistance. Biomed. Pharmacother. 2024;178:117119.
34. Bourang S, Jahanbakhsh Godehkahriz S, Asghari Zakaria R, Parsa H, Noruzpuor M. Green synthesis of iron oxide, copper, zinc oxide and silver nanoparticles from aqueous extract of *F. vulgare* and evaluation of their structural and antimicrobial properties. Agric Biotechnol. 2024;16(3):60-88.
35. Yusefi M, Shameli K, Su Yee O, Teow S-Y, Hedayatnasab Z, Jahangirian H, Webster TJ, Kuča K. Green synthesis of Fe_3O_4 nanoparticles stabilized by a Garcinia mangostana fruit peel extract for hyperthermia and anticancer activities. Int J Nanomedicine. 2021:2515-2532.
36. Abebe DG, Kandil R, Kraus T, Elsayed M, Merkel OM, Fujiwara T. Three-layered biodegradable micelles prepared by two-step self-assembly of PLA-PEI-PLA and PLA-PEG-PLA triblock copolymers as efficient gene delivery system. Macromol Biosci. 2015;15(5):698-711.
37. Afrouz M, Ahmadi-Nouraldinvand F, Ajirlu YY, Arabnejad F, Eskanlou H, Yaghoubi H. Preparation and characterization of PLA-PEG/Chitosan-FA/DNA for gene transfer to MCF-7 cells. Med. Drug Discov. 2022;15:100138.
38. Bourang S, Noruzpour M, Azizi S, Yaghoubi H, Ebrahimi HA. Synthesis and *in vitro* characterization of PCL-PEG-HA/FeCo magnetic nanoparticles encapsulating curcumin and 5-FU. Nanomed J. 2024;11(2).
39. Solano-Gálvez SG, Abadi-Chiriti J, Gutiérrez-Velez L, Rodríguez-Puente E, Konstat-Korzenny E, Álvarez-Hernández D-A, Franyuti-Kelly G, Gutiérrez-Kobeh L, Vázquez-López R. Apoptosis: activation and inhibition in health and disease. Med Sci. 2018;6(3):54.
40. Calahorra J, Blaya-Cánovas JL, Castellini-Pérez O, Aparicio-Puerta E, Cives-Losada C, Marin JJ, Rementeria M, Cara FE, López-Tejada A, Griñán-Lisón C. Unlocking the effective alliance of β-lapachone and hydroxytyrosol against triple-negative breast cancer cells. Biomed Pharmacother. 2024;174:116439.
41. Mokhtarieh AA, Lee J, Kim S, Lee MK. Preparation of siRNA encapsulated nanoliposomes suitable for siRNA delivery by simply discontinuous mixing. BBA-Biomembranes. 2018;1860(6):1318-1325.
42. Le-Vinh B, Le N-MN, Nazir I, Matuszczak B, Bernkop-Schnürch A. Chitosan based micelle with zeta potential changing property for effective mucosal drug delivery. Int J Biol Macromol. 2019;133:647-655.
43. Martinez-Morales F, Alonso-Castro AJ, Zapata-Morales JR, Carranza-Álvarez C, Aragon-Martinez OH. Use of standardized units for a correct interpretation of IC50 values obtained from the inhibition of the DPPH radical by natural antioxidants. Chem Pap. 2020;74:3325-34.
44. González-Larraza PG, López-Goerne TM, Padilla-Godínez FJ, González-López MA, Hamdan-Partida A, Gómez E. IC50 evaluation of platinum nanocatalysts for cancer treatment in fibroblast, HeLa, and DU-145 cell lines. ACS omega. 2020;5(39):25381-25389.
45. Mohammed A-SY, Dyab AK, Taha F, Abd El-Mageed AI. Encapsulation of folic acid (vitamin B9) into sporopollenin microcapsules: Physico-chemical characterisation, *in vitro* controlled release and photoprotection study. Mater Sci Eng C. 2021;128:112271.
46. Zheng D, Giljohann DA, Chen DL, Massich MD, Wang X-Q, Iordanov H, Mirkin CA, Paller AS. Topical delivery of siRNA-based spherical nucleic acid nanoparticle conjugates for gene regulation. Spherical Nucleic Acids: Jenny Stanford Publishing; 2020;1605-1623.
47. Ge X, Chen L, Zhao B, Yuan W. Rationale and application of PEGylated lipid-based system for advanced target delivery of siRNA. Front Pharmacol. 2021;11:598175.
48. Sako M, Song F, Okamoto A, Koide H, Dewa T, Oku N, Asai T. Key determinants of siRNA delivery mediated by unique pH-responsive lipid-based liposomes. Int J Pharm. 2019;569:118606.
49. Ebadi M, Rifqi Md Zain A, Tengku Abdul Aziz TH, Mohammadi H, Tee CAT, Rahimi Yusop M. Formulation and characterization of Fe_3O_4@ PEG nanoparticles loaded sorafenib; molecular studies and evaluation of cytotoxicity in liver cancer cell lines. Polymers. 2023;15(4):971.
50. Bourang S, Jahanbakhsh-Godekahriz S, Asghari-Zakaria R, Parsa-Khankandi H, Noruzpour M, Calahorra J. Evaluation of antioxidant properties of essential oil, aqueous extract and metal nanoparticles biosynthesized from *F. vulgare* and their anticancer effect on two breast cancer cell lines (Sum-159, Hs-578T). Agric Biotechnol. 2024;16(1):235-66.
51. Heidari R, Khosravian P, Mirzaei SA, Elahian F. siRNA delivery using intelligent chitosan-capped mesoporous silica nanoparticles for overcoming multidrug resistance in malignant carcinoma cells. Sci Rep. 2021;11(1):20531.